

# Aperture-synthesis imaging with the LBT: Reconstruction of diffraction-limited images from LBT LINC-NIRVANA data using the Richardson-Lucy and regularized Building Block method

Karl-Heinz Hofmann<sup>a</sup>, Thomas Driebe<sup>a</sup>, Mathias Heininger<sup>a</sup>, Dieter Schertl<sup>a</sup>, Gerd Weigelt<sup>a</sup>

<sup>a</sup>Max-Planck-Institute for Radioastronomy, Auf dem Hügel 69, Bonn, Germany

## ABSTRACT

The regularized and space-variant Building Block method<sup>1</sup> allow the reconstruction of diffraction-limited aperture-synthesis images from Large Binocular Telescope (LBT) LINC-NIRVANA data. Images with the diffraction-limited resolution of a 22.8 m single-dish telescope can be reconstructed if raw images are taken at several different hour angles. Computer-generated and laboratory LBT interferograms were simulated that are similar to the data which can be obtained with the LINC-NIRVANA beam combiner instrument. From the simulated interferograms, diffraction-limited images were reconstructed with the regularized Building Block method, which is an extension of the Building Block method.<sup>2</sup> We compare the Building Block reconstructions to images obtained with the Richardson-Lucy (RL) method<sup>3,4</sup> and the Ordered Subsets Expectation Maximization (OSEM) method.<sup>5,6</sup> Our image reconstruction studies were performed with computer-simulated J-band and laboratory H-band raw data of a galaxy with simulated total magnitudes of J = 16 to 18 and H = 16 to 19, respectively. One of the faintest structures in the images has a brightness of J~25. The simulated reference stars within the isoplanatic patch have magnitudes of J = 20 - 21 and H = 19. All three methods are able to reconstruct diffraction-limited images of similar quality.

**Keywords:** interferometry, high angular resolution, image reconstruction

## 1. INTRODUCTION

The raw images obtained with LINC-NIRVANA,<sup>7,8</sup> the optical/NIR beam combiner of the Large Binocular Telescope, will have, in one direction, the spatial resolution equivalent to a diffraction-limited 8.4 m single-dish telescope, and in the orthogonal direction, that of a 22.8 m telescope. The LBT<sup>9,10</sup> with its two 8.4 m mirrors is being built on Mt. Graham, Arizona. From exposures taken at a few different hour angles, reconstructed images with a spatial resolution which reaches that of a 22.8 m single-dish telescope can be obtained.

First aperture synthesis studies were presented by Hege et al.<sup>11</sup> and Angel et al.<sup>12</sup>. Reinheimer et al.<sup>13</sup> have investigated the reconstruction of diffraction-limited images from computer-simulated LBT speckle interferograms. Diffraction-limited images were reconstructed with the Bispectrum Speckle Interferometry method and the Building Block method. Correia & Richichi,<sup>14</sup> Bertero & Boccacci,<sup>6</sup> Carbillet et al.,<sup>15</sup> Correia et al.,<sup>16</sup> and Anconelli et al.<sup>17</sup> have investigated the deconvolution of Adaptive Optics (AO) corrected LBT raw images with the Richardson-Lucy algorithm and related methods.

We have applied an extension of the Building Block method<sup>1</sup> to LINC-NIRVANA raw data obtained from computer and laboratory simulations. The main features of the extension are a regularization scheme to improve the quality of the reconstructed images and a method to reconstruct images in the case of *space-variant* point-spread functions (PSFs) in the large LINC-NIRVANA field-of-view (FOV) of  $\sim 10''$ . Space-variant deconvolution is important for the optimal reconstruction of images obtained with the LINC-NIRVANA instrument.

---

Further author information: (Send correspondence to K.-H. Hofmann)  
K.-H. Hofmann: E-mail: khh@mpifr-bonn.mpg.de

## 2. THE REGULARIZED BUILDING BLOCK METHOD

In this section, we discuss the regularized Building Block method<sup>1,2</sup> which we used for the image reconstruction studies described in Sects. 3 and 4. The intensity distribution of an object  $o(x)$  can be described as a sum of many building blocks (e.g.  $\delta$ -functions). The goal of the BB method is the calculation of a high-resolution aperture synthesis image that is equal to the convolution of  $o(x)$  with the diffraction-limited point-spread function (PSF) of a large single-dish telescope; for instance, a 22.8 m aperture in the case of the LBT. The BB method iteratively produces images  $o_k(x)$  ( $k=1,2,\dots$ ) by adding one or more building blocks  $\delta(x-x_0)$  at each iteration step  $k$ . The goal is to find an image  $o_k(x)$  which minimizes the  $\chi^2$  function

$$Q[o_k(x)] := \int \left| \frac{o_k(x) \otimes p(x) - i(x)}{\sigma(x)} \right|^2 dx, \quad (1)$$

where  $x$  is a 2-dimensional space coordinate,  $\otimes$  denotes the convolution operator,  $p(x)$  is the sum LBT PSF discussed in Sect. 3.1 (i.e., the sum of the PSFs taken at different hour angles), and  $\sigma(x)$  denotes the Poisson and detector noise in the image  $i(x)$  which is the sky background-subtracted sum LBT raw image (i.e., the sum of the individual raw images taken at different hour angles; see Sect. 3.1). The functions  $i(x)$ ,  $p(x)$ , and  $o_k(x)$  are normalized to an integral intensity of 1.

The new building block added to  $o_k(x)$  to obtain  $o_{k+1}(x)$  is positioned at a particular coordinate  $x = x_0$  in  $o_k(x)$ . Since  $o_k(x)$  and  $o_{k+1}(x)$  are normalized to an integral intensity of 1,  $o_{k+1}(x)$  is given by

$$o_{k+1}(x) = \frac{n_k \cdot o_k(x) + \delta(x-x_0)}{n_k + 1} \approx o_k(x) + \frac{1}{n_k} \cdot \delta(x-x_0), \quad (2)$$

where  $\delta(x-x_0)$  is the new building block, and  $n_k$  denotes the number of building blocks of  $o_k(x)$ . Since  $n_k \gg 1$  after a large number  $k$  of iteration steps, the right side of Eq. (2) holds. In this realization of the BB method all building blocks have the same amplitude. Another approach is to fit simultaneously the amplitude and position of the new building block as mentioned in Hofmann & Weigelt.<sup>2</sup> For the position  $x_0$  of the new building block, a value is chosen that leads to an image which minimizes the  $\chi^2$  function  $Q[o_k(x) + 1/n_k \cdot \delta(x-x_0)]$ . For a large number  $k$  of iterations, each contribution  $1/n_k \cdot \delta(x-x_0)$  is very small. Therefore,  $Q[o_k(x) + 1/n_k \cdot \delta(x-x_0)]$  can be approximated by a Taylor expansion:

$$\begin{aligned} Q[o_k(x) + 1/n_k \cdot \delta(x-x_0)] &\approx Q[o_k(x)] + \frac{1}{n_k} \cdot \frac{\partial Q}{\partial o_k(x_0)} = \\ &= Q[o_k(x)] + \frac{2}{n_k} \cdot \frac{o_k(x_0) \otimes p(x_0) - i(x_0)}{\sigma^2(x_0)} \otimes p(-x_0). \end{aligned} \quad (3)$$

Eq. (3) shows that the  $\chi^2$  function  $Q$  is minimized by adding a positive (negative) building block at that position in  $o_k(x)$  where the function  $\partial Q/\partial o_k(x_0)$  has its absolute minimum (maximum). Reconstructions are often improved by simultaneously adding positive and negative building blocks per iteration step. Negative building blocks are only added, if the positivity constraint is not violated.

One well-known technique that can lead to improved reconstructions is the *regularization* of the fitting procedure: instead of searching for the global minimum of the  $\chi^2$  function  $Q$ , the minimum of  $Q$  must be estimated under certain conditions. One such condition is the smoothness of the reconstructed image, expressed, for example, by the entropy function<sup>18</sup>

$$H[o(x)] := \int o(x) \cdot \ln[o(x)] dx, \quad (4)$$

where  $\ln$  is the natural logarithm. The goal is to find the image that minimizes the function

$$J[o(x)] := Q[o(x)] + \mu \cdot H[o(x)], \quad (5)$$

where  $Q[o(x)]$  is the  $\chi^2$  function given in Eq. (1), and  $\mu$  is a Lagrange multiplier which can be roughly estimated as described in Appendix A of Hofmann et al.<sup>1</sup> To find the image that minimizes  $J[o(x)]$ , the Taylor expansion

of  $J[o_k(x) + 1/n_k \cdot \delta(x - x_0)]$  around  $o_k(x)$  is required:

$$\begin{aligned} J[o_k(x) + 1/n_k \cdot \delta(x - x_0)] &\approx J[o_k(x)] + \frac{1}{n_k} \cdot \frac{\partial J}{\partial o_k(x_0)} = \\ &= J[o_k(x)] + \frac{1}{n_k} \cdot \left\{ \frac{\partial Q}{\partial o_k(x_0)} + \mu \cdot \frac{\partial H}{\partial o_k(x_0)} \right\}, \end{aligned} \quad (6)$$

where  $\partial H/\partial o_k(x_0)$ , according to Eq. (4), is given by

$$\frac{\partial H}{\partial o_k(x_0)} = \ln[o_k(x_0)] + 1. \quad (7)$$

Eq. (6) shows that the function  $J$  is minimized by adding a positive (negative) building block at the position in  $o_k(x)$  where the function  $\partial J/\partial o_k(x_0)$  has its absolute minimum (maximum). Applications of this BB method with regularization are presented in the next two sections.

### 3. APERTURE-SYNTHESIS IMAGING

#### 3.1. Computer simulation of the interferograms

The LBT raw images  $i'_j(x)$  are modeled as

$$i'_j(x) = o(x) \otimes p_j(x) + b_j(x) + r_j(x), \quad (8)$$

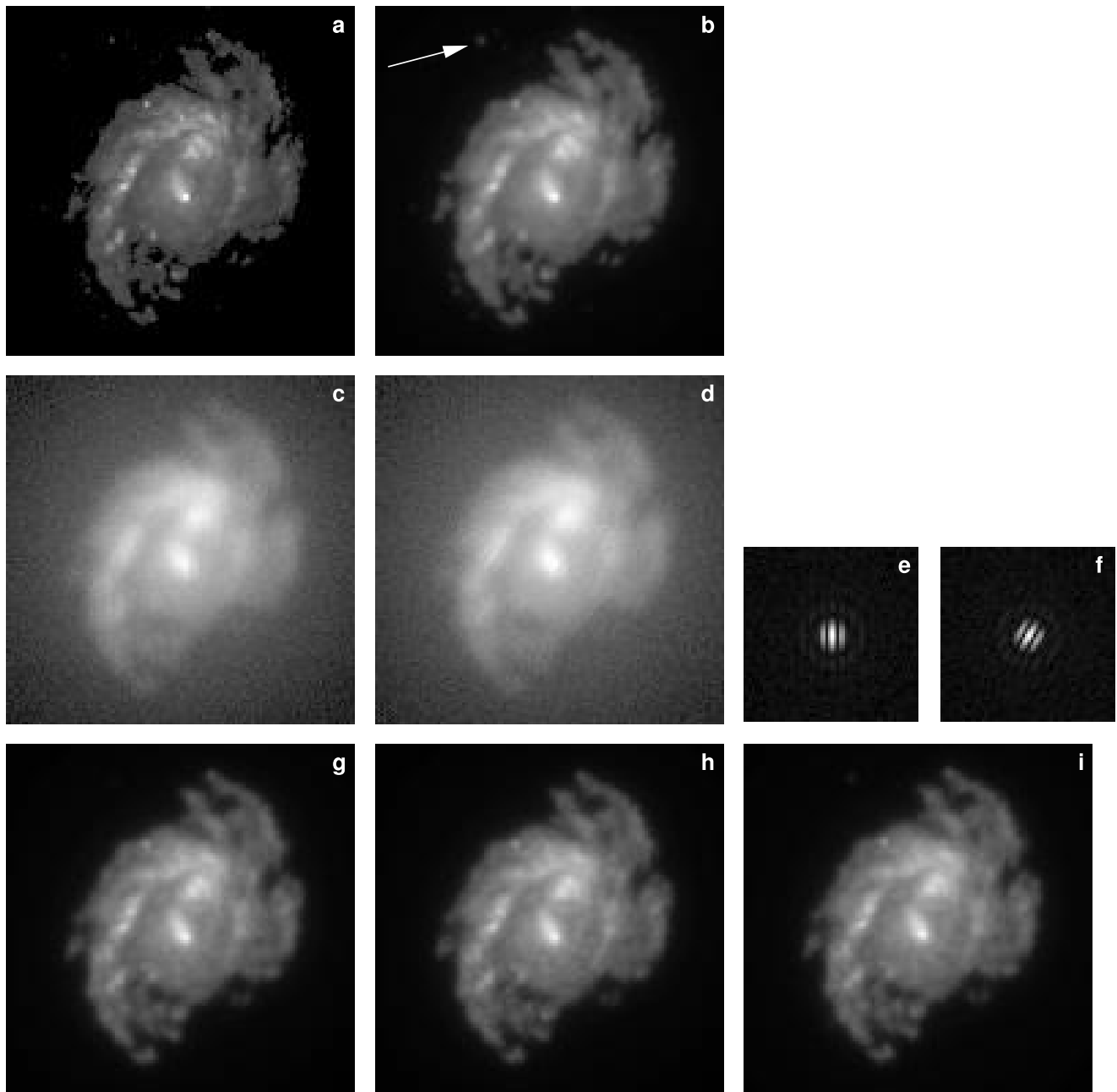
where  $o(x)$  denotes the intensity distribution of the object;  $i'_j(x)$  and  $p_j(x)$  with  $j = 1, \dots, m$  are the  $m$  LBT raw images and PSFs, respectively, recorded at  $m$  different pupil position angles;  $b_j(x)$  describes the sky background, and  $r_j(x)$  is the noise caused by the detector (mainly read-out noise) as well as the limited number of photons of the object and the sky background. The subtraction of the sky background yields the input images  $i_j(x) = o(x) \otimes p_j(x) + r_j(x)$ . The OSEM method uses the individual images  $i'_j(x)$  (including sky background) and the sky background-subtracted PSFs  $p_j(x)$  (without clipping negative values) as input. The RL method uses the sum  $i'(x)$  of all LBT raw images  $i'_j(x)$  (with sky background) and the sky background-subtracted sum PSF  $p(x)$  of the corresponding LBT raw PSFs  $p_j(x)$  as input data. The Building Block method uses the sum  $i(x)$  of all sky background-subtracted LBT raw images  $i_j(x)$ , the sum  $p(x)$  of the corresponding sky background-subtracted LBT raw PSFs  $p_j(x)$ , and the sum  $b(x)$  of all sky backgrounds  $b_j(x)$  as input data.

Figure 1 presents the results of our image reconstruction experiments using the RL, OSEM, and BB methods. In these computer experiments, a computer-generated galaxy with a total J-band magnitude of 17<sup>m</sup> was chosen. The faint, star-like structure in the upper left corner of Fig. 1b (marked by an arrow) has a simulated J magnitude of 25.2<sup>m</sup>. The magnitudes of the reference stars in the simulation are 20.0<sup>m</sup>, 20.5<sup>m</sup>, 20.5<sup>m</sup>, and 21.0<sup>m</sup>, respectively.

Figure 1 shows (a) the computer-generated reference object, (b) the reference object convolved with a theoretical PSF corresponding to a single-dish 22.8 m pupil, (c, d) two of the six raw images simulated for two different pupil position angles (0° and 30°), and (g-i) the results of the image reconstruction experiments obtained with the three different deconvolution methods.

The raw images are obtained through convolution of the object intensity distribution (Fig. 1a) with the simulated LBT PSFs (for example, Figs. 1e, f), addition of sky background, and simulation of photon and detector read-out noise. LBT PSFs with partial AO corrections (Strehl ratio  $\sim 30\%$ ) were simulated in the following way:

- (1) a phase screen was generated which produces speckle interferograms with one dominant diffraction-limited core surrounded by many faint speckles, which correspond to the speckle halo caused by partial AO corrections;
- (2) an intermediate short-exposure LBT PSF was obtained by calculating the squared Fourier transform of the complex amplitude transmission of the phase screen multiplied with the LBT pupil function;
- (3) the summation of a large number of intermediate short-exposure LBT PSFs, derived from many different phase screens, yielded the LBT PSF for the corresponding position angle and exposure time (see Figs. 1e, f).



**Figure 1.** Aperture-synthesis imaging with the LBT (all images are shown on the same scale). **a:** test object (based on the HST image of NGC 3504); **b:** object from panel (a) convolved with the PSF of a simulated diffraction-limited 22.8 m telescope; **c, d:** computer-simulated LBT raw images of the object (simulated total magnitude  $J=17.0^m$ , sky background  $J=16.0^m$  per arcsec square, read-out noise of  $11 e^-$  rms, pupil position angles  $0^\circ$  and  $30^\circ$ ); **e, f:** LBT PSFs for position angles  $0^\circ$  and  $30^\circ$ . These PSFs are derived from four unresolved stars in the vicinity of the target. The brightness of these reference stars ranges from  $J=20.0^m$  to  $21.0^m$ ; **g, h, i:** diffraction-limited images reconstructed from 6 LBT raw images (taken with pupil position angles of  $0^\circ$ ,  $30^\circ$ ,  $60^\circ$ ,  $90^\circ$ ,  $120^\circ$ , and  $150^\circ$ , two of which are shown in panels c and d) and the corresponding 6 LBT PSFs (two of which are shown in panels e and f) using the RL (g), the OSEM (h), and the BB (i) methods; the faint star-like structure in the upper left corner of panels a and b has a brightness of  $J=25.2^m$  (marked by an arrow in panel b). The restoration errors are 5.37% (g), 5.61% (h), and 5.20% (i) (see text for details).

**Table 1.** Parameters of the computer-simulated LBT raw images (Fig. 1).

Primary mirror size	8.4 m
Primary mirror center-to-center distance	14.4 m
Optical transmission	0.5
Quantum efficiency of the detector	0.6
Number of pixels per frame	2048 × 2048
Pixel size	5.0 mas
read-out noise	11 $e^-$
Central wavelength / bandwidth	1.25/0.3 $\mu\text{m}$
Object type	extended galaxy based on the HST image of NGC 3504
Total object magnitude	$m_J = 17.0$
Magnitudes of the 4 reference stars in the 2048×2048 pixel FOV	$m_J = 20.0, 20.5, 20.5, 21.0$
Magnitude of the sky background per square arcsec	$m_J = 16.0$
Position angles of the pupil axis	0°, 30°, 60°, 90°, 120°, 150°
Strehl ratio	0.3
Exposure time	600 sec for each of the above six pupil position angles

For the computer experiments shown in Fig. 1, we simulated PSFs and raw images of the object corresponding to six different pupil position angles equally spaced between 0° and 180°. We assumed an integration time of 600s per position angle, a 30% efficiency (optics and detector), a read-out noise of 11 electrons rms, and a J-band sky background brightness of 16<sup>m</sup> per arcsec square. The simulated photon noise of the six LBT raw images of the galaxy (two are shown Figs. 1c and d) corresponds to a total magnitude of the whole galaxy of J=17.0<sup>m</sup>. The 6 LBT PSFs (two are displayed in Figs. 1e and f) were derived from four unresolved stars located close to the target and with distances to the center of the target ranging between 2.6" and 5.8". The parameters of the computer simulation described here are listed in Table 1.

### 3.2. Image reconstruction using the RL, OSEM, and BB methods

The LBT raw images and LBT PSFs were preprocessed in the following way:

- (1) The PSFs for the deconvolution process were obtained by adding up the PSFs of the four re-centered, unresolved reference stars surrounding the target.
- (2) The sky background was estimated and subtracted from the LBT PSFs (without clipping negative values); for the BB method, the sky background was subtracted from the LBT raw images of the target (without clipping negative values);
- (3) In the Fourier transform of each individual LBT raw image, all elements outside the uv-coverage corresponding to a given pupil function were set to zero in order to reduce the noise.
- (4) Co-adding of the re-centered LBT raw images recorded at all six pupil position angles and preprocessed as described in (2) and (3) yields the input data for the RL and BB methods. The LBT raw images were

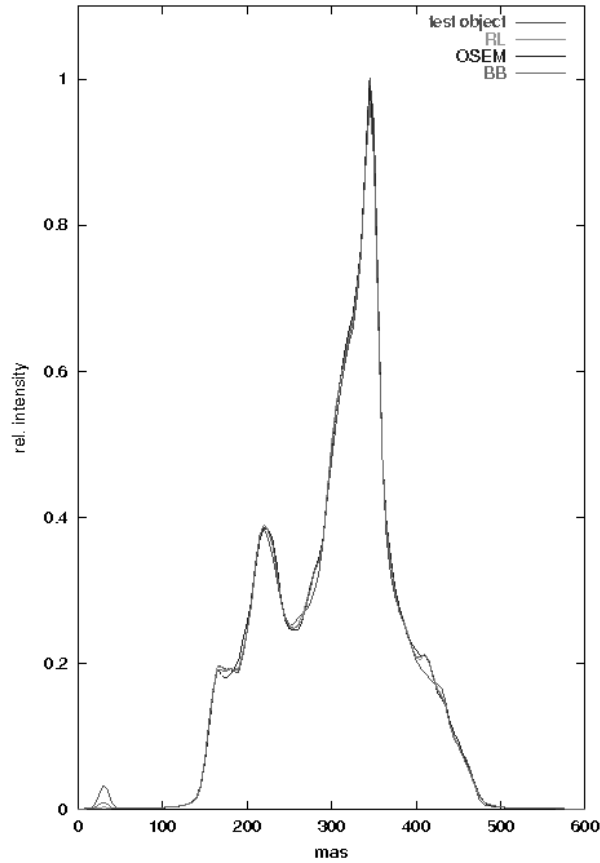


**Figure 2.** Intensity distribution along a line through the nucleus and the faint star-like object (upper left corner in Fig. 1b) for the test object (Fig. 1b; red), the RL reconstruction (Fig. 1g; green), the OSEM reconstruction (Fig. 1h; blue), and the BB reconstruction (Fig. 1i; pink).

re-centered using the shift-vectors determined from the re-centering procedure of the surrounding reference stars for the derivation of the LBT-PSFs (1). OSEM uses the six individual preprocessed LBT raw images and LBT PSFs as input data.

The reconstruction methods RL, OSEM, and BB iteratively reconstruct diffraction-limited images from the LBT raw data. For the RL and OSEM deconvolution experiments presented in this paper, the publicly available AIRY package<sup>16</sup> (version 2.0) was used with the estimated sky background level as an additional input value. The BB image reconstruction experiments presented in this paper were performed with the algorithm and the regularization scheme outlined in Sect. 2.

Figures 1g-i show the images derived from six LBT raw images (see examples in Figs. 1c and d) and the corresponding six LBT PSFs (two are shown in Figs. 1e and f) by using the three image reconstruction methods RL, OSEM, and BB, respectively.

In our simulations, the restoration error, which is a measure of the quality of the image reconstruction, is defined as

$$\rho := \frac{\sqrt{\int |o_k(x) \otimes p'(x) - o(x) \otimes p'(x)|^2 dx}}{\sqrt{\int |o(x) \otimes p'(x)|^2 dx}}, \quad (9)$$

where  $o(x) \otimes p'(x)$  is the computer object convolved with the theoretical diffraction-limited PSF  $p'(x)$  of a hypothetical 22.8 m single-dish telescope (Fig. 1b), and  $o_k(x) \otimes p'(x)$  (Figs. 1g-i) is the reconstruction convolved

with the same PSF  $p'(x)$ . Both images are normalized according to  $\int o_k(x) \otimes p'(x) dx = \int o(x) \otimes p'(x) dx$ . In the definition of  $\rho$ , the reconstruction  $o_k(x)$  and the reference object  $o(x)$  are convolved with  $p'(x)$  since the goal of interferometric LBT imaging is usually to obtain an image with the diffraction-limited resolution of a hypothetical 22.8 m single-dish telescope.

The average restoration errors of the three reconstructions were determined to be  $5.41 \pm 0.10\%$  (RL),  $5.58 \pm 0.08\%$  (OSEM), and  $5.30 \pm 0.10\%$  (BB). These errors were calculated from 10 raw data sets (see parameters in Table 1) that were statistically independent with respect to photon and detector read-out noise and the phase screens simulating partial AO. Figure 2 shows intensity cuts along a line through the nucleus and the faint star-like object (upper left corner in Fig. 1b) for the test object (Fig. 1b; red), the RL reconstruction (Fig. 1g; green), the OSEM reconstruction (Fig. 1h; blue), and the BB reconstruction (Fig. 1i; pink).

In order to study the dependence of the quality of the reconstructions on the brightness of the astronomical target, we performed two additional experiments with the computer-generated galaxy shown in Fig. 1a and total J-band magnitudes of  $16^m$  and  $18^m$ . All other parameters of the computer-simulated LBT raw images were the same as for the experiment shown in Fig. 1 (see parameters in Table 1). The average restoration errors of the reconstructions obtained with the RL, OSEM, and BB methods are listed in Table 3.2. As in the case of object brightness  $J=17^m$ , all three methods yield reconstructions of similar quality and restoration errors.

**Table 2.** Restoration errors of the reconstructions using the galaxy test object shown in Fig. 1 (see also Table 1) with total magnitudes of  $J=16.0^m$ ,  $J=17.0^m$ , and  $J=18.0^m$ . The restoration errors listed are averages of 10 statistically independent LBT data sets (see text).

J magnitude	RL	OSEM	BB
16.0	$4.29 \pm 0.14\%$	$4.81 \pm 0.10\%$	$4.09 \pm 0.14\%$
17.0	$5.41 \pm 0.10\%$	$5.58 \pm 0.08\%$	$5.30 \pm 0.10\%$
18.0	$7.38 \pm 0.22\%$	$7.63 \pm 0.16\%$	$7.43 \pm 0.22\%$

## 4. LABORATORY LBT SIMULATIONS

### 4.1. Laboratory simulated interferograms

Simulated LBT LINC-NIRVANA data of a galaxy (see Fig. 3a) were recorded with a laboratory LBT simulator and a HAWAII-1 array camera. The simulator consists of the lenses of an imaging setup, a slide which contains the laboratory object and the reference star, a rotatable pupil mask which simulates the LBT pupil, and a rotating phase screen that allows the simulation of partial AO correction.

The laboratory data was taken in the H band. Images of the object and one unresolved star were simultaneously recorded (see Figs. 3b and c). For each image reconstruction experiment, images were taken with 6 different pupil position angles (see Table 4.1). Data sets with simulated total galaxy magnitudes of  $H = 16.2^m$ ,  $17.1^m$ ,  $17.8^m$ , and  $19.1^m$  were recorded. For each of the 4 object brightnesses, 10 statistically independent data sets were recorded, which allowed the determination of the error of the restoration errors. Sky background was simulated as thermal background by heating the LBT pupil mask. The object and the PSF were recorded with a simulated full 22.8 m pupil to be able to compare the reconstructions of the LINC-NIRVANA simulations with full-pupil images. A summary of the parameters of the laboratory experiments is given in Table 4.1.

The simulated PSFs consist of a dominant diffraction-limited 3-fringe core and an extended AO speckle halo (see Figs. 3b and c). The speckle contrast in this halo is high if the exposure times are short compared to the simulated speckle life time and low (as in our experiments) if the exposure times are long compared to the speckle life time. The Strehl ratio simulated in this experiment was 0.10.

The raw laboratory images were preprocessed in the following way:

- (1) The images were flat-fielded, and pixel bias and bad pixel effects were corrected.
- (2) The sky background was estimated by fitting the measured sky background to the actual background in the data.

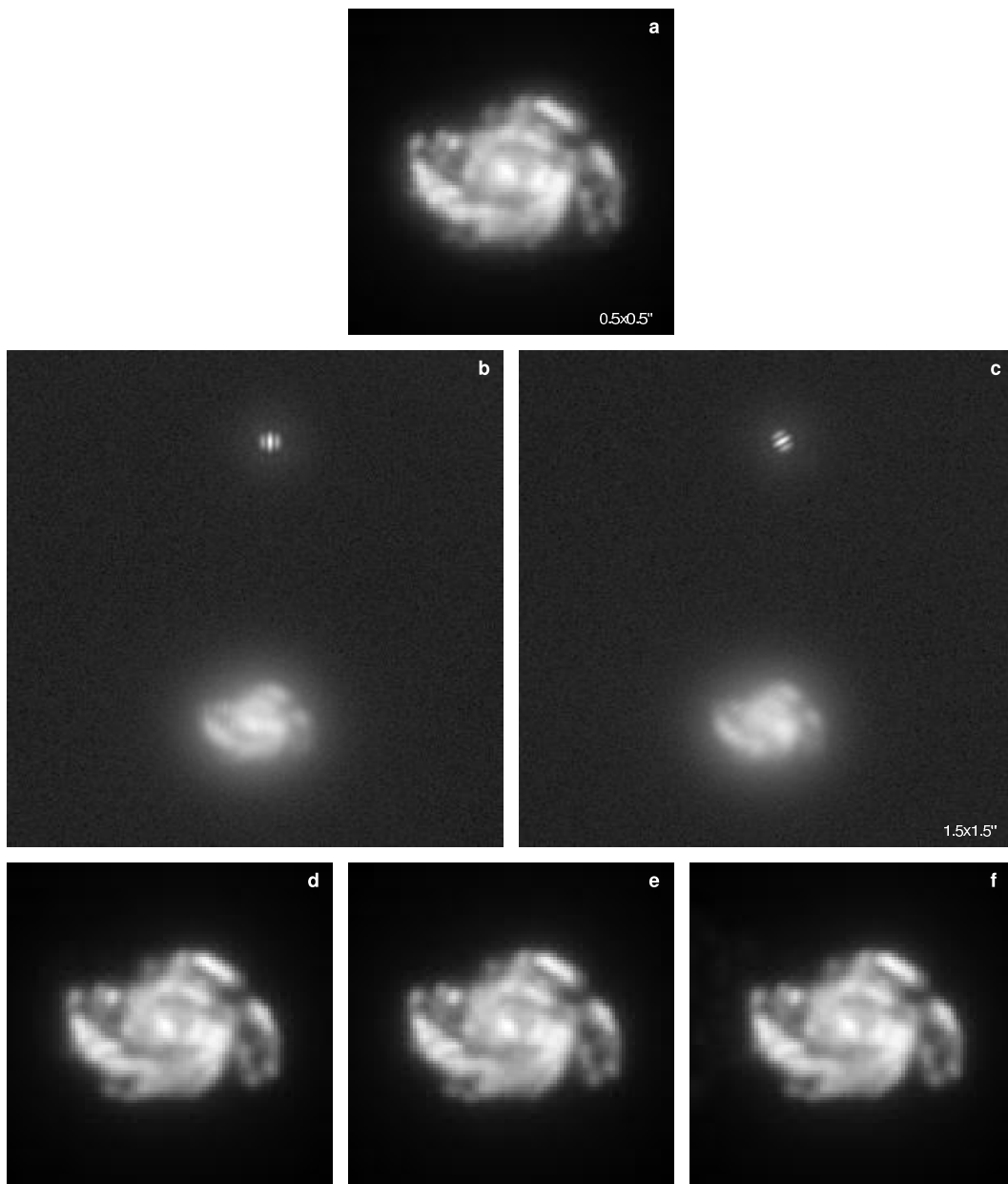


**Figure 3.** Image reconstruction from laboratory LBT data using the RL, OSEM, and BB methods. **a:** Test object (galaxy) used for the laboratory experiment (simulated resolution corresponding to a diffraction-limited 22.8 m single-dish telescope). **b, c:** Laboratory LBT raw images and PSFs for pupil position angles  $0^\circ$  and  $60^\circ$ . **d, e, f:** Diffraction-limited reconstructions derived from 6 LBT raw images (total magnitude  $H = 16.2^m$ ) using the RL (d) , OSEM (e), and BB methods (f). The restoration errors are 6.85% (d), 6.76% (e), and 6.23% (f).

**Table 3.** Parameters of our laboratory simulation.

Optical transmission	0.5
Quantum efficiency of the detector	0.6
Pixel size	18.0 $\mu\text{m}$
Number of detector pixels	512 $\times$ 512
RON	17 $e^-$
Central wavelength / filter width	1.65/0.3 $\mu\text{m}$
total object magnitudes	$m_{\text{H}} = 16.2/17.1/17.8/19.1$
PSF star magnitude	$m_{\text{H}} = 19.2$
Magnitude of the sky background per square arcsec	$m_{\text{H}} = 14.0$
Pupil position angles	$0^\circ, 30^\circ, 60^\circ, 90^\circ, 120^\circ, 150^\circ$
Simulated Strehl ratio	0.10
Exposure time per pupil position angle	600 sec

(3) To reduce the noise in the individual data corresponding to a certain hour angle, all elements in the Fourier transform outside the uv-coverage of the simulated LBT pupil were set to zero. As discussed in Appendix B of Hofmann et al.,<sup>1</sup> this Fourier-masking reduces the restoration error.

(4) For the RL and BB methods, all 6 images corresponding to the different hour angles were co-added. For OSEM, the individual images were used.

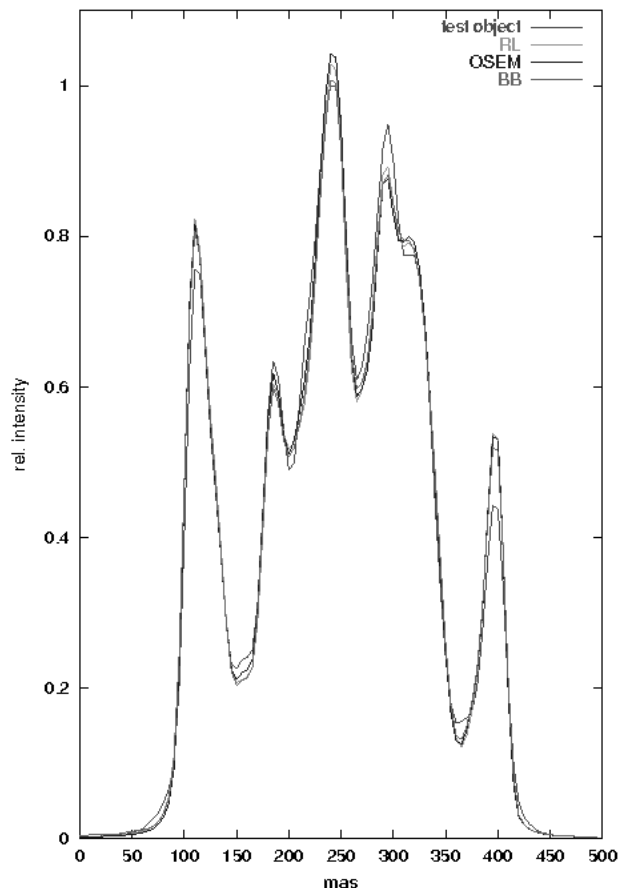
#### 4.2. RL, OSEM, and BB method reconstructions

Figure 3 summarizes the results of one of the laboratory LINC-NIRVANA image reconstruction experiments. In this experiment the following parameters were simulated: total magnitude of the galaxy H = 16.2<sup>m</sup>, magnitude of the reference star H = 19.1<sup>m</sup>, and sky background H = 14.0<sup>m</sup> per square arcsec. Figure. 3a shows an image of the laboratory object taken with a simulated 22.8 m single dish pupil. Figures. 3b and c show two of the six simulated raw images (pupil position angle = 0° and 60°). Figures. 3d-f show the images reconstructed with the RL, the OSEM, and the BB methods. The restoration errors obtained for the four different object magnitudes H = 16.2<sup>m</sup>, 17.1<sup>m</sup>, 17.8<sup>m</sup>, and 19.1<sup>m</sup> are summarized in Table 4.2.

As in the case of the computer simulations discussed in the previous section, the reconstructed images obtained with the three methods RL, OSEM, and BB are of similar quality. For a given object brightness all restoration errors agree within the error bars. As expected, in general the restoration quality becomes worse with decreasing object brightness (from ~5% for H=16<sup>m</sup> to ~13% for H=19<sup>m</sup>). Figure 4 shows intensity cuts along a horizontal line through the nucleus for the test object (Fig. 3a; red), the RL reconstruction (Fig. 3d; green), the OSEM reconstruction (Fig. 3e; blue), and the BB reconstruction (Fig. 3f; pink).

### 5. CONCLUSIONS

We presented an extended version of the Building Block algorithm for the reconstruction of diffraction-limited images from data obtained with the LBT LINC-NIRVANA instrument. The main features of this extension are a *regularization* scheme and a method to handle *space-variant* PSFs (described in Hofmann et al.<sup>1</sup>). We carried out a large number of image deconvolution experiments to study the quality of images reconstructed from simulated LINC-NIRVANA data with the regularized Building Block method. We compared the Building Block reconstructions to images obtained with the Richardson-Lucy method and the Ordered Subsets Expectation



**Figure 4.** Intensity cuts along a horizontal line through the nucleus for the test object (Fig. 3a; red), the RL reconstruction (Fig. 3d; green), the OSEM reconstruction (Fig. 3e; blue), and the BB reconstruction (Fig. 3f; pink).

**Table 4.** Restoration errors of the reconstructions obtained with the RL, OSEM, and BB methods from the Fourier-masked laboratory LBT raw images

H magnitude	RL	OSEM	BB
16.2	$5.74 \pm 0.56\%$	$5.56 \pm 0.55\%$	$5.44 \pm 0.33\%$
17.1	$7.53 \pm 0.54\%$	$7.18 \pm 0.53\%$	$6.86 \pm 0.43\%$
17.8	$9.40 \pm 0.58\%$	$9.11 \pm 0.50\%$	$8.38 \pm 0.49\%$
19.1	$13.53 \pm 0.65\%$	$13.52 \pm 0.63\%$	$12.93 \pm 0.37\%$

Maximization method, and determined the restoration error as a function of the object’s brightness. We find that all three methods are able to reconstruct diffraction-limited images with almost the same quality. Our image reconstruction studies were performed with computer-simulated and laboratory raw data of a galaxy with simulated total magnitudes of  $J = 16^m$  to  $18^m$ , and  $H = 16^m$  to  $19^m$ , respectively. One of the faintest structures in the images has a brightness of  $J \sim 25^m$ . The simulated reference stars have magnitudes in the ranges of  $J = 20^m$  to  $21^m$  and  $H = 19^m$ .

## REFERENCES

1. K.-H. Hofmann, T. Driebe, M. Heininger, D. Schertl, and G. Weigelt, “Reconstruction of aperture-synthesis images from lbt linc-nirvana data using the richardson-lucy and space-variant building block method,” *A&A* **444**, pp. 983–993, 2005.

2. K.-H. Hofmann and G. Weigelt, "Iterative image reconstruction from the bispectrum," *A&A* **278**, pp. 328–339, 1993.
3. W. Richardson, "Bayesian-based iterative method of image restoration," *J. Opt. Soc. Am.* **62**, pp. 55–59, 1972.
4. L. Lucy, "An iterative technique for the rectification of observed distributions," *AJ* **79**, pp. 745–754, 1974.
5. H. Hudson and R. Larkin, "...," *IEEE Trans. Med. Imag.* **13**, pp. 601–609, 1994.
6. M. Bertero and P. Boccacci, "Application of the os-em method to the restoration of lbt images," *A&AS* **144**, pp. 181–186, 2000.
7. T. Herbst, R. Raggazzoni, D. Andersen, and et al., "Linc-nirvana, a fizeau beam combiner for the large binocular telescope," in *Interferometry for Optical Astronomy II*, W. A. Traub, ed., *Proc. SPIE* **4838**, pp. 456–465, 2003.
8. T. Herbst, R. Raggazzoni, A. Eckart, and G. Weigelt in *Ground-based Instrumentation for Astronomy*, A. Moorwood and M. Iye, eds., *Proc. SPIE* **5492**, p. 1045, 2004.
9. J. Hill and P. Salinari in *Large Ground-based Telescopes*, J. Oschmann and L. M. Stepp, eds., *Proc. SPIE* **4837**, p. 140, 2003.
10. J. Hill and P. Salinari in *Ground-based Telescopes*, J. Oschmann, ed., *Proc. SPIE* **5489**, p. 603, 2004.
11. E. Hege, J. Angel, M. Cheselka, and M. Lloyd-Hart, "Simulation of aperture synthesis with the large binocular telescope," in *Optical Aperture Synthesis*, J. Gonglewski, ed., *Proc. SPIE* **2566B**, pp. 144–155, 1995.
12. J. Angel, J. Hill, P. Strittmatter, P. Salinari, and G. Weigelt, "Interferometry with the large binocular telescope," in *Advanced Technology Optical/IR Telescopes VI*, R. D. Reasenberg, ed., *Proc. SPIE* **3352**, p. 881, 1998.
13. T. Reinheimer, K.-H. Hofmann, M. Schoeller, and G. Weigelt, "Speckle masking interferometry with the large binocular telescope," *A&AS* **121**, pp. 191–199, 1997.
14. S. Correia and A. Richichi, "Interferometric imaging tests for the large binocular telescope," *A&AS* **141**, pp. 301–311, 2000.
15. M. Carbillet, S. Correia, P. Boccacci, M. Bertero, and L. Fini, "Restoration of interferometric images ii. the case-study of the large binocular telescope," *A&A* **387**, pp. 744–757, 2002.
16. S. Correia, M. Carbillet, P. Boccacci, M. Bertero, and L. Fini, "Restoration of interferometric images i. the software package airy," *A&A* **387**, pp. 733–743, 2002.
17. B. Anconelli, M. Bertero, P. Boccacci, M. Carbillet, and H. Lanteri, "Restoration of interferometric images iii. efficient richardson-lucy methods for linc-nirvana data reduction," *A&A* **430**, pp. 731–738, 2005.
18. F. Wahl, *Digitale Bildverarbeitung*, Springer Verlag, Heidelberg-New-York-Tokio, 1984.